Memorias del Congreso ASME USB 2011:
IX CONGRESO ANUAL DE INGENIERÍA ASME USB 2011
03, 04 Y 05 de junio, 2011, Caracas - Venezuela

AUSB2011-11030104

COMPARATIVE STUDY OF RANS TURBULENCE MODELS FOR IMPINGING JET SIMULATIONS

Vittori F.
Simón Bolívar University
Department of Transport and Energy Conversion
Caracas, Venezuela
vittorifelpe@yahoo.com

Rojas-Solórzano L.
Simón Bolívar University
Department of Transport and Energy Conversion
Caracas, Venezuela

Pavageau M.
Ecole des Mines d'Albi
Campus Jarlard
81013 ALBI
France

ABSTRACT

Impinging plane jets are flow configurations with applications in many fields. The ability of several turbulence models to simulate this kind of flow was assessed. The numerical results were compared with the data of Cooper et al. (1993) for Re=7.0 104 and a jet nozzle aspect ratio H/D=6, and Re=2.3 104 and H/D=2. The SST, RSM-ε and RSM-BSL turbulence models were chosen because of their capability to predict flows with high streamline curvature and their expected good accuracy on near wall flow. The results show that the SST and RSM- ε perform better than the RSM-BSL in the prediction of the mean velocity profiles in the wall-jet and impact zone. The profiles of turbulent energy were particularly difficult to reproduce. All the turbulence models considered here exhibit a similar behavior with respect to the profiles of turbulent energy. The paper shows again the complexity of turbulent impinging jets and the relevant open challenges in CFD.

INTRODUCTION

Over the past two decades, the use of Computational Fluid Dynamics (CFD) codes has become a rather common approach to solve a wide variety of industrial problems involving for example multiphase flows in large pipes, flows around turbine blades, water flows in open channels, etc. Computational Fluid Dynamics allow to obtain approximate numerical solutions to complex flow situations with sometimes a very good accuracy making possible the routinely use of CFD codes.

Nowadays, in the development phase of a new product, experimental tests are more and more often replaced by CFD analysis to minimize design time and costs related to the building of experimental facilities and instrumentation.

Solving turbulence motion in flows using CFD is based on three general approaches. The Reynolds Averaged Navier-Stokes (RANS) approach may be the most popular approach because of the large number of turbulence models developed within the frame of this formulation of the equations of turbulence. It offers good results for a large variety of engineering situations. It is widely applied because simple PC clusters are usually sufficient to run the required simulations. Direct Numerical Simulation (DNS) is the most accurate method. However, it requires a lot of computational resources like mainframes or high-performance clusters to run simulations at high Reynolds numbers. Large Eddy Simulation (LES) corresponds to an approach intermediate between RANS and DNS in terms of computational cost and accuracy.

Even though RANS models are the most used in engineering, they do not always provide acceptable solutions. Therefore, in all engineering applications it is mandatory to first validate the turbulence models to be used to guarantee a correct solution [2].

The validation process consists usually in determining if the numerical model is able to reproduce the main patterns of a selected actual reference flow [2]. It has to be performed before proceeding to a complete CFD parameter study on a given case study.

This study addresses CFD analysis of plane impinging jets. This apparently simple flow configuration is actually not so easy to reproduce numerically because it involves simultaneously several basic flows including free jet, wall jets, a stagnation area with strong velocity gradients (see fig. 1) and even a cross-flow (the latter will not be taken into account in this study) [3].

Cooper et al. (1993) performed experiments to capture the main behavior and fluid patterns of round plane impinging jet to offer data for validation purposes. They noticed important aspects: (a) the turbulence energy along the jet axis is created by normal straining; (b) the r.m.s. of the fluctuating velocity normal to the impingement wall is larger than that of the parallel component; (c) turbulence length scales near the wall is strongly affected by the jet initial turbulence; and finally (d) the convective transport of turbulent energy near the stagnation point (Impact Zone) has important contribution as in the parallel flow to wall.

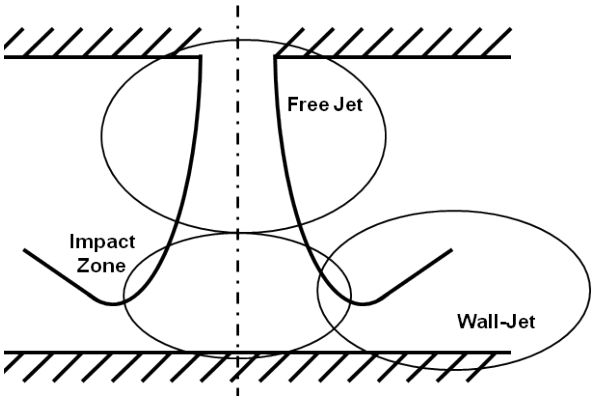

Figure 1. Impinging Jet flow composition

Craft et al. (1993) performed a validation of four RANS turbulence models: k-ε and three versions of the Reynolds Stress Model or Second Moment Closure (RSM or SMC), modified to capture the fluctuating quantities at the stagnation point and in the wall jet through an additional term called wall-reflection. Their results show that the eddy viscosity model over-predicts the turbulence and the velocities, while the RSM model gives much better results from an engineering point of view; however, none of the models under scrutiny were able to reproduce accurately the turbulent field. Later, Dianat et al. (1996) did a comparison study between an RSM model with the wall-reflection term and another RSM model without this term. Their results show a superior prediction of normal-to-wall velocity fluctuations and shear stress by the RSM model with the wall-reflection term.

With a different approach, Beaubert et al. (2003) applied LES simulations to reproduce experiments on plane impinging jets at two Reynolds numbers. The results show a favorable agreement with the experiments. The authors note that their model is accurate enough to allow studying and getting a better understanding about the physics of the flow especially in the impact zone, which is typically very difficult to observe in experiments.

Although LES is more accurate than RANS models, Rhea et al. (2009) showed that nevertheless RSM models offered good results. The differences they obtained in their validation work on impinging jets proved to be smaller than with two-equation RANS models.

Finally, Fernández et al. (2007) showed that the RANS two-equation model k-ε was able to predict mean velocities and turbulent kinetic energy with an acceptable accuracy for engineering applications. However, the model was not able to predict the jet expansion and the flow in the impact region correctly.

The scope of the work presented here was to assess the capability of RANS turbulence models to reproduce impinging jets with sufficient accuracy for engineering applications. The numerical results were compared against the experiments of Cooper et al. (1993).

Successful RANS approaches could be further used to optimize the performance of many processes or machines, like for example the vertical take-off of some jet planes like the Harrier V-8 where in the earlier stage of the elevation the turbine expels the gases vertically on the floor. This take-off mode is very difficult to model and requires more research as mentioned by Saddington et al. (2005).

NOMENCLATURE

U	Velocity in the flow direction (m/s)
V	Velocity normal to flow direction (m/s)
ρ	Fluid density [air 1.185kg/ m^3] (kg/m^3)
t	Time (s)
p	Pressure (N/m^2)
g	Gravity acceleration (m/s^2)
μ	Fluid viscosity (Ns/m^2)
μ_t	Turbulent viscosity (Ns/m^2)
δ	Kronecker Delta function (dimensionless)
P_{ij}	Shear turbulence production ($kg/m/s^3$)
τ	Molecular stress tensor (N/m^2)
H	Distance between the impingement plate and the jet nozzle (m)
D	Nozzle diameter (m)
x	Coordinate (m) in a Cartesian frame
u	Fluctuating velocity of the mean flow (m/s)
k	Turbulent kinetic energy (m^2/s^2)
a_1	Model constant (dimensionless)
ω	Turbulent dissipation frequency (s^{-1})
S	Strain rate magnitude (N/m^2)
F_1, F_2	Blending functions (dimensionless)
ε	Turbulent dissipation rate (m^2/s^3)

Subscripts

i	i´th direction
t	Turbulent
b	Bulk

MATHEMATICAL MODEL

The Reynolds Averaged Navier-Stokes equations in steady state, for an incompressible Newtonian fluid are solved numerically. The governing equations may be written as

$$\frac{\partial U_j}{\partial x_j} = 0 \quad (1)$$

$$\frac{\partial \rho U_i}{\partial t} + \frac{\partial}{\partial x_j}\left(\rho U_i U_j\right) - \frac{\partial}{\partial x_j}\left[\mu\left(\frac{\partial U_i}{\partial x_j} + \frac{\partial U_j}{\partial x_i}\right)\right] = -\frac{\partial p}{\partial x_i} - \frac{\partial}{\partial x_j}\left(\rho\overline{u_i u_j}\right) \quad (2)$$

To solve this set of mathematical equations it is required to approximate the Reynolds Stress tensor through a turbulence model. This work considers an eddy viscosity model and a Reynolds Stress Models.

Eddy viscosity turbulence model

In this group of turbulence models, one of the most successful models is the Shear Stress Transport (SST) one, which takes advantage of the k-ε model for free stream flows and the k-ω for an accurate solution of boundary layers and reattachment lengths. This hybrid method has proved to be superior to other two-equation models according to many documented experiences [10].

The eddy viscosity hypothesis assumes that Reynolds stresses can be related to mean velocity gradients and turbulent viscosity by the gradient diffusion hypothesis, i.e.:

$$-\rho\overline{u_\iota u_J} = \mu_t\left(\frac{\partial U_i}{\partial x_j}+\frac{\partial U_j}{\partial x_i}\right)-\frac{2}{3}\delta_{ij}\rho k \quad (3)$$

Where k=$\overline{u_\iota u_\iota}/2$ and$\mu_t = \frac{\rho a_1 k}{max(a_1\,\omega, SF_2)}$. The values of k and ω are computed from the solution of the modeled transport equations:

$$\frac{\partial\rho k}{\partial t}+\frac{\partial}{\partial x_j}(\rho U_i k)-\frac{\partial}{\partial x_j}\left[\left(\mu+\frac{\mu_t}{\sigma_{k3}}\right)\frac{\partial k}{\partial x_j}\right]=P_k-\acute{\beta}\rho k\omega \quad (4)$$

$$\frac{\partial\rho\omega}{\partial t}+\frac{\partial}{\partial x_i}(\rho U_i\omega)-\frac{\partial}{\partial x_j}\left[\left(\mu+\frac{\mu_t}{\sigma_{\omega 3}}\right)\frac{\partial\omega}{\partial x_j}\right]=(1-F_1)2\rho\frac{1}{\sigma_{\omega 2}\omega}\frac{\partial k}{\partial x_j}\frac{\partial\omega}{\partial x_j}+\alpha_3\frac{\omega}{k}P_k-\acute{\beta_3}\rho\omega^2 \quad (5)$$

The term is the blending function between the models, where F1 is equal to 1 near the surface and decreases to 0 outside the boundary layer. The coefficients are linear combination of the corresponding k –ε2 and –ω1 models:

$$\emptyset_3 = F_1\emptyset_1+(1-F_1)\emptyset_2 \quad (6)$$

The coefficients are β =0.09; α1=5/9; β1=0.075; σk1=2; σω1=2; α2=0.44; β2=0.0828; σk2=1; σω2=1/0.856. The function F1 and F2 are based on the distance to the nearest surface and on the flow variables by:

$$F_1 = \tanh\left(arg_1^4\right) \quad (7)$$

$$arg_1 = min\left(max\left(\frac{\sqrt{k}}{\beta'\omega y},\frac{500\vartheta}{y^2\omega}\right),\frac{4\rho k}{CD_{k\omega}\sigma_{\omega 2}y^2}\right) \quad (8)$$

$$CD_{k\omega} = max\left(2\rho\frac{1}{\sigma_{\omega 2}\omega}\frac{\partial k}{\partial x_j}\frac{\partial\omega}{\partial x_j},1\times10^{-10}\right) \quad (9)$$

$$F_2 = \tanh\left(arg_2^2\right) \quad (10)$$

$$arg_2 = max\left(\frac{\sqrt{k}}{\beta'\omega y},\frac{500\vartheta}{y^2\omega}\right) \quad (11)$$

Production limiters

In order to avoid the build-up of turbulent kinetic energy in stagnation regions, so-called "limiters" are available for the production term of turbulence Pk. The standard turbulence production due to viscous forces for incompressible fluid is given by:

$$P_k = \mu_t\frac{\partial U_i}{\partial x_j}\left(\frac{\partial U_i}{\partial x_j}+\frac{\partial U_j}{\partial x_i}\right) \quad (12)$$

While, Menter´s formulation [10] introduces the next changes:

$$P_k = \min\left(P_k, C_{lim}\rho\varepsilon\right) \quad (13)$$

$$P_k = \mu_t S^2 \quad (14)$$

$$S=\sqrt{2S_{ij}S_{ij}}, S_{ij}=\frac{1}{2}\left(\frac{\partial U_i}{\partial x_j}+\frac{\partial U_j}{\partial x_i}\right) \quad (15)$$

The coefficient Clim is named Clip Factor and is 10 for ω models.

The other limiter is the Kato and Launder [10] replacement of the production term by:

$$P_k = \mu_t S\Omega \quad (16)$$

$$\Omega=\sqrt{2\Omega_{ij}\Omega_{ij}}, \Omega_{ij}=\frac{1}{2}\left(\frac{\partial U_i}{\partial x_j}-\frac{\partial U_j}{\partial x_i}\right) \quad (17)$$

Where Ωij is the vorticity tensor.

Reynolds Stress Model (RSM)

This turbulence model is based on the solution of a transport equation for each of the six components of the Reynolds stress tensor, with an additional expression for the turbulent dissipation rate. The modeled Reynolds stress transport equation and the energy dissipation rate used in the present work may be written as:

$$\frac{\partial\rho\overline{u_\iota u_J}}{\partial t}+\frac{\partial}{\partial x_k}\left(\rho U_k\overline{u_\iota u_J}\right)-\frac{\partial}{\partial x_k}\left[\left(\mu+\frac{2}{3}C_S\rho\frac{k^2}{\varepsilon}\right)\frac{\partial\overline{u_\iota u_J}}{\partial x_k}\right]=P_{ij}-\frac{2}{3}\delta_{ij}\rho\varepsilon+\varphi_{ij} \quad (18)$$

$$\frac{\partial\rho\varepsilon}{\partial t}+\frac{\partial}{\partial x_k}\left(\rho U_k\varepsilon\right)-\frac{\partial}{\partial x_k}\left[\left(\mu+\frac{\mu_t}{\sigma_{\varepsilon RS}}\right)\frac{\partial\varepsilon}{\partial x_k}\right]=\frac{\varepsilon}{k}(C_{\varepsilon 1}P-C_{\varepsilon 2}\rho\varepsilon) \quad (19)$$

The coefficients are CS= 0.22; σεRS=1.1; Cε1=1.45; Cε2=1.9. Where Pij is the production term and φij is the pressure-strain correlation according to Launder, Reece and Rodi [10], which may be represent by:

$$P_{ij} = -\rho\overline{u_\iota u_k}\frac{\partial U_j}{\partial x_k}-\rho\overline{u_J u_k}\frac{\partial U_i}{\partial x_k} \quad (20)$$

$$\varphi_{ij} = -C_1\rho\frac{\varepsilon}{k}\left(\overline{u_\iota u_J}-\frac{2}{3}\delta_{ij}k\right)-C_2\left(P_{ij}-\frac{2}{3}P\delta_{ij}\right) \quad (21)$$

The values of the coefficients are C1=1.8 and C2=0.6, and P is given by 0.5Pii.

Additionally, the RSM models have a variant based on the same scope of the SST turbulence approximation called RSM-Base Line (RSM-BSL), which consists in a blended function for the dissipation equation, transforming it in a ε relation for the outer flow region and in a ω equation for a more accurate near-wall treatment. The modeled RSM-BSL equation and the new transport equation of energy dissipation may be written as:

$$\frac{\partial\rho\overline{u_\iota u_J}}{\partial t}+\frac{\partial}{\partial x_k}\left(\rho U_k\overline{u_\iota u_J}\right)-\frac{\partial}{\partial x_k}\left[\left(\mu+\frac{\mu_t}{\sigma_k}\right)\frac{\partial\overline{u_\iota u_J}}{\partial x_k}\right]=P_{ij}-\frac{2}{3}\delta_{ij}\rho\omega k\beta'+\varphi_{ij} \quad (22)$$

$$\frac{\partial\rho\omega}{\partial t}+\frac{\partial}{\partial x_k}(\rho U_k\omega)-\frac{\partial}{\partial x_k}\left[\left(\mu+\frac{\mu_t}{\sigma_{\omega 3}}\right)\frac{\partial\omega}{\partial x_k}\right]=(1-F_1)2\rho\frac{1}{\sigma_2\omega}\frac{\partial k}{\partial x_k}\frac{\partial\omega}{\partial x_k}+\alpha_3\frac{\omega}{k}P_k-\beta_3\rho\omega^2 \quad (23)$$

Where the coefficients are calculated in the same way as for equation 6, using the corresponding constants for ω: $\alpha 1=0.553$; $\beta 1=0.075$; $\sigma 1=2$; and for ε zone: $\alpha 2=0.44$; $\beta 2=0.0828$; $\sigma 2=0.856$. The term F1 is calculated as in equations (7), (8) and (9).

In the present work, all the simulations were carried out in isothermal conditions. Thus no heat transfer was calculated.

All the turbulence models described above used an automatic wall function that allows calculating boundary layers as a function of the mesh size close to the wall [10].

GEOMETRY AND BOUNDARY CONDITIONS

The reference experimental set up is shown in fig. 2. The data taken from the work of Cooper et al. (1993) correspond to Re=70000 for $H/D_1=6$ (D_1=101.6mm) and Re=23000 for $H/D_2=2$ (D_2=26mm).

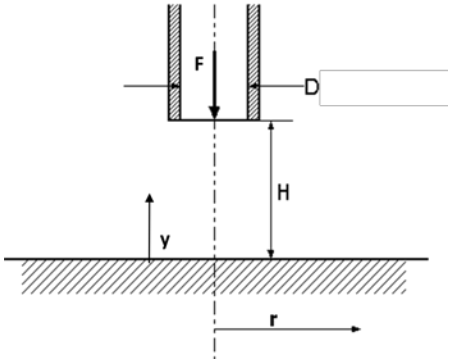

Figure 2. Discharge pipe over the impinging surface.

The simulations were performed in a two dimensional plane, taking advantage of the axial symmetry of the flow [1]. Fig. 3 shows the H/D=2 computational domain with the respective boundary conditions. The velocity profile at the discharge inlet was established through the Nikuradse´s velocity profile for turbulent flow in smooth pipe at the respective Reynolds number. At the impact plane, a not slip condition was applied. The open surfaces were treated as constant pressure and stress-free sections.

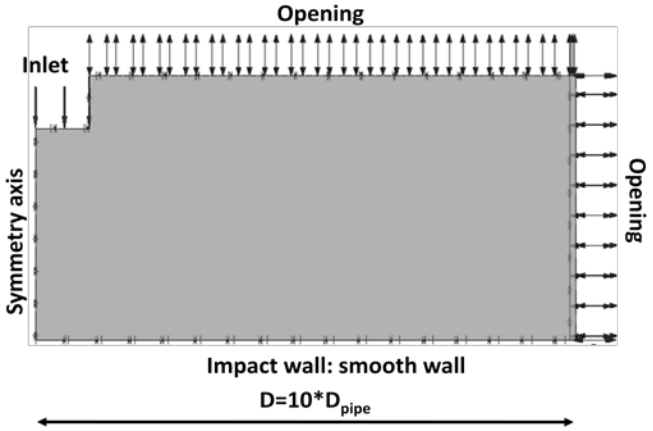

Figure 3. Boundary conditions for 2D axisymmetric flow.

The numerical solutions were obtained using a structured hexahedral grid. The governing equations were discretized using the element-based finite volume method for which the domain is discretized through a finite element mesh used to construct finite volumes employed to conserve mass and momentum. The model was run using ANSYS-CFX v.12.

The numerical solutions presented below were obtained from a mesh of 41084 and 168435 elements for the H/D=2 and H/D=6 geometries, respectively. Tests were performed in both cases with meshes comprising twice as less and twice as much elements. No differences were noticed so that the results presented here can be considered as grid-independent.

ANSYS-CFX solves the governing equations for u, v, w, p in a coupled manner, as a single system. This solution approach uses a fully implicit discretization scheme of the equations. Two operations are performed to solve the problem; a construction of non-linear equation into a linearized solution matrix and then, the linear equations are solved using an Algebraic Multigrid method. The multigrid process involves carrying out early iterations on a fine mesh and later iterations on progressively coarser virtual ones. The results are then transferred back from the coarsest mesh to the original fine mesh minimizing numerical oscillations and giving more robustness to the method. The momentum, mass and turbulence equations were solved with a 2nd order accurate scheme through a higher order upwind scheme for the advective terms and central difference discretization for the remaining terms.

RESULTS AND DISCUSSION

H/D=2 Configuration, Re=23000

The fig. 4 shows the profile of the r.m.s fluctuation of the axial component of velocity in the impact zone for the 5 turbulence models explored in this work. The results are compared with the experimental data of Cooper et al. (1993). The distance y is counted from the impingement plate. Between 0,2D to 0.4D from the wall, the turbulence approximation is in good agreement with the experiment. A discrepancy of the order of 16% with experiments is observed at y/D=0.15 with the SST model with the Kato and Launder modification. The best match occurs for the classic SST with a 0.8% difference. The other models match the experiments within that range. However, from 0 to 0.2D from the wall, all the simulations diverge from the experiment due to wall effects. The experimental turbulent fluctuations drop to zero turbulence transferring its energy to the main flow that behaves like a non-rotational flow as mentioned by Craft *et al* (1993) and Dianat *et al* (1996).

The RSM models produce excessive turbulent energy; even the RSM-BSL is unable to control the production of turbulence although it was developed to capture close-to-wall phenomena as the ω-model in the SST model. In the stagnation region the RSM-BSL offers slightly better value than the classic RSM, but the two-equation models offers better predictions of the turbulent profile.

With its hybrid formulation the SST model offers better results than the predictions of Craft *et al.* (1993) who showed that the k-ε model was over predicting the turbulence quantities in the stagnation region by almost a factor four due to the fact

Reynolds stress (eqn. 3) tends to increase proportionally to turbulent kinetic energy. Therefore, it is important to remark that the ω and the μ_t formulations of the SST had been improved than those of the k-ε standard model for the turbulent predictions.

Additionally the production limiters have proven to be effective for the control of turbulent energy generation on the impact region. The method with the clip factor offers the best approximation when CL=3. For higher values of CL, the turbulence peak increases for the standard SST. For valus of CL smaller than 3, unrealistic flow patterns are obtained. Thus, it is important to keep in mind that this method, which is an artificial way to get better approximations, can also lead to non-physics results.

The Kato and Launder (SST-KL) modification offers a constant profile not affected by the wall as a consequence of the vorticity term added to the production term. The *u´u´* Reynolds stress decreases very slowly on approaching the wall. The Kato and Launder modification does not lead to any overestimate of the turbulence level in the flow region considered here because the production of turbulent energy is zero in the stagnation region due to the irrotational characteristics of the model (vorticity is set to zero in eqns. 16 and 17).

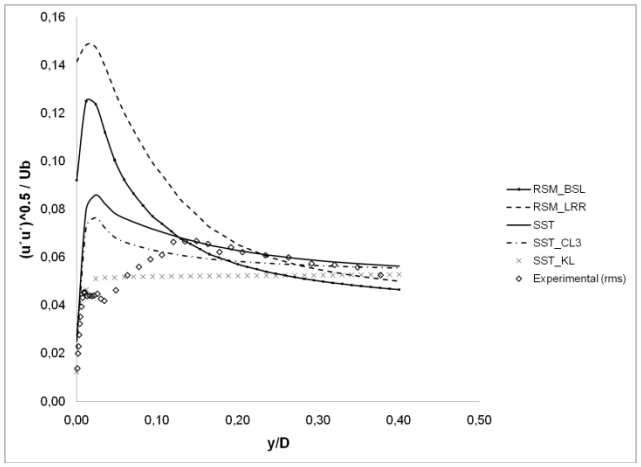

Figure 4. Fluctuating r.m.s. velocity profile and Reynolds stresses profiles on the symmetry line in the stagnation region.

Figure 5 shows the velocity magnitude at a distance r/D=0,5 from the symmetry axis. The velocity is calculated with the parallel (U, mean flow direction) and normal (V, normal flow direction) to the wall components, respectively. For this distance, the normal component has a significant contribution due to the effect of the stagnation region were the flow direction changes from perpendicular to the surface to parallel to it. All the velocity profiles almost superimpose depicting a good approximation to the experimental data.

The major departure from experiments is reported by the SST and SST-KL with a deviation of 8.8% at y=0,4D. The RSM models offer better results than the two-equation models. They predict the maximum velocity near the surface within no more than 5% of the experimental value. Even far from the wall, the numerical profiles are in rather good agreement with the experiments even though all the SST models underpredict the magnitude of velocity far from the wall while, on the contrary, they tend to overpredict the velocity close to it. Note that the fluid velocity does not vanish close to the wall due to a vertical component and an apparent slip velocity [1].

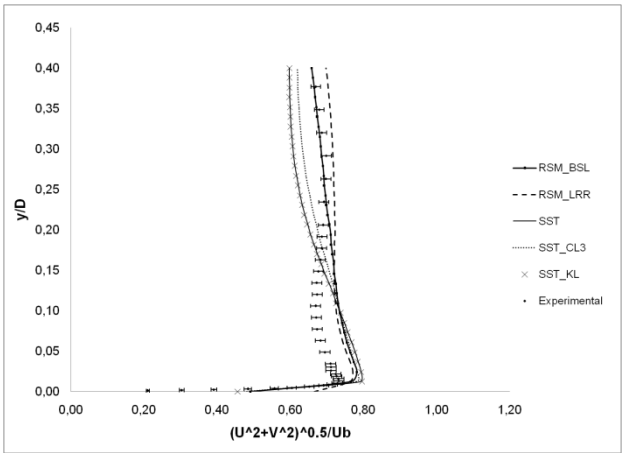

Figure 5. Mean velocity profile at r/D=0,5.

Figure 6 shows the velocity magnitude at a distance r/D=1 from the symmetry axis. At this position the velocity is dominated by the parallel-to-wall component of velocity with practically no contribution of the normal-to-wall component of velocity. All the models predict very well the position and the magnitude of the maximum of velocity near the wall. The worst fit is observed far from the wall for the SST-KL model.

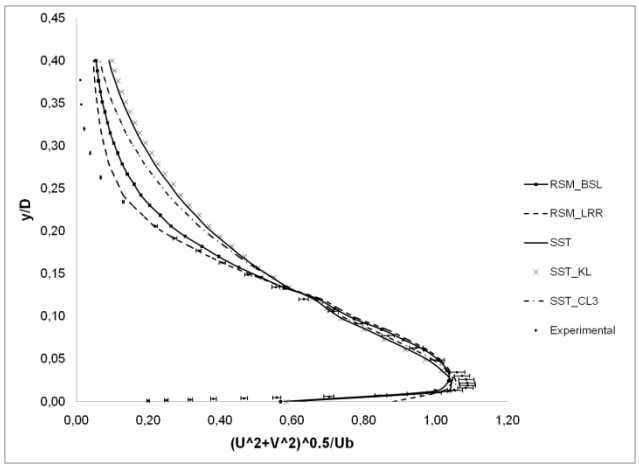

Figure 6. Mean velocity profile at r/D=1.

Figure 7 shows at r/D=2,5 that the velocity profile returned by the SST models better match the experimental profile. The RSM tends to seriously under-predict the position and magnitude of the maximum of velocity.

At r/D=2,5 the velocity magnitude has decreased by a factor 2 with respect to its value at r/D=1. Actually, the peak of maximum velocity occurs precisely at r/D=1. It is thus where the wall-jet region can be considered to begin.

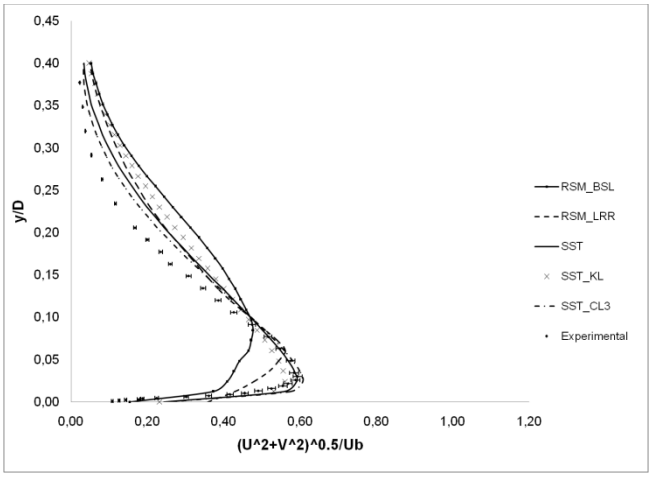

Figure 7. Mean velocity profile at r/D=2,5.

Figure 8 shows the r.m.s. velocity fluctuation of the wall-jet and the corresponding Reynolds stress. The RSM models were able to capture the profile behavior near the wall but completely under-predict the turbulent stresses away from the surface. Meanwhile, the SST models return profiles that do not match in detail the experimental one. However, the predicted order of magnitude of the r.m.s. of the velocity fluctuation is correct in first approximation.

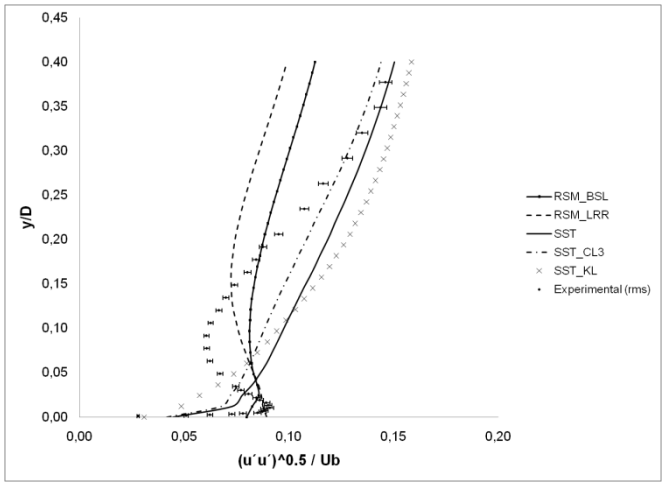

Figure 8. Development of the r.m.s. velocity fluctuations and Reynolds Stress in the wall-jet at r/D=0,5.

Figure 9 exhibits characteristics similar to those of figure 8. Numerical results, however, better approximate the experimental maximum value of turbulent stress and its position above the wall. The RSM models consistently over-predict the experimental results, while the SST tends to under-predict them. The most difficult to simulate is the experimental turbulence pattern at y/D=0.05 where the $(u´u´)^{1/2}/U_b$ has a falls and a peak that correspond to the maximum mean velocity of the wall-jet.

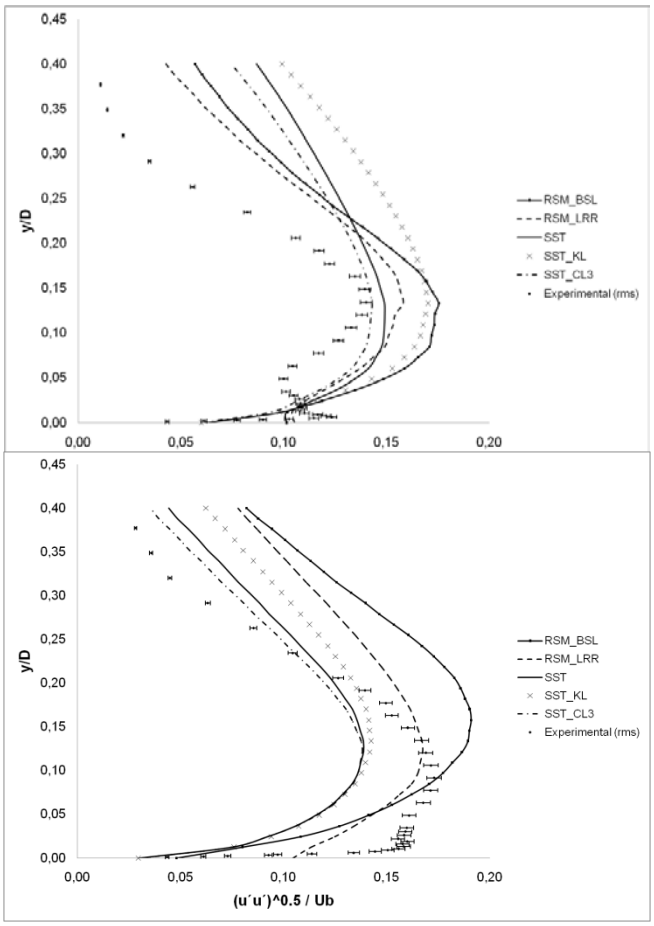

Figure 9. Profiles of the parallel to wall r.m.s. velocity fluctuation in the mean flow at r/D=1 and r/D=2.5 respectively.

H/D=6 Configuration, Re=70000

Figure 10 shows the r.m.s of the normal to wall component of velocity. The same comments as for the case H/D=2 can be made. The SST-KL model avoids any excessive production of turbulence due to the irrotational feature imposed to the flow in the stagnation region. The relevant experimental data for $Re=7.0\ 10^4$ exhibit larger values than at $Re=2.3\ 10^4$. However, the normalized profiles have the same behavior: for $0.2<y/D<0.4$, the r.m.s of u' is constant. For $0<y/D<0.2$ the r.m.s. of u' exhibits a decrease and an increase until a peak located almost at the wall. This shows that a change of Re (in the range of values considered here) does not affect the turbulence behavior in the impact zone. Only the magnitude of phenomena is altered.

Figure 11 shows the profiles of velocity magnitude at r/D=0.5, 1.5 and 3. The numerical approximation was similar to the H/D=2 case, but now the RSM models diverge much more from the experiments, at r/D=1.5, there is a difference of about 30% between the maximum velocity value of the wall-jet reported by the RSM_BSL and the experimental result. Finally, at r/D=3, the RSM models predict a uniform wall-jet velocity profile with a non defined peak velocity close to the wall as seen in the experiments. Meanwhile, the SST models offer better results at the three radial positions capturing similar velocity profile. Additionally the production limiters modifications were not significant in the velocity fields.

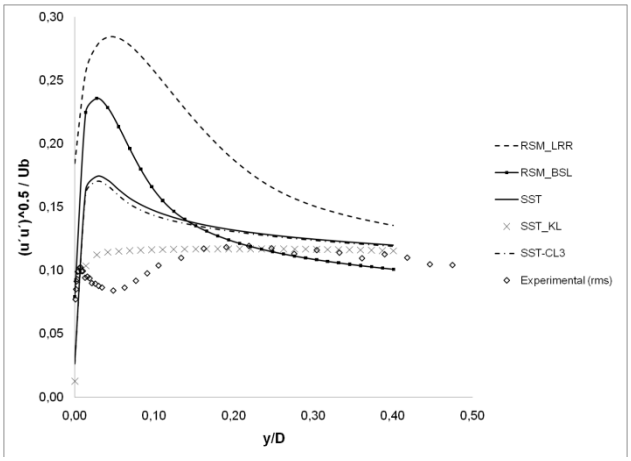

Figure 10. Fluctuating r.m.s. velocity profile and Reynolds stresses profiles along the jet axis in the stagnation region.

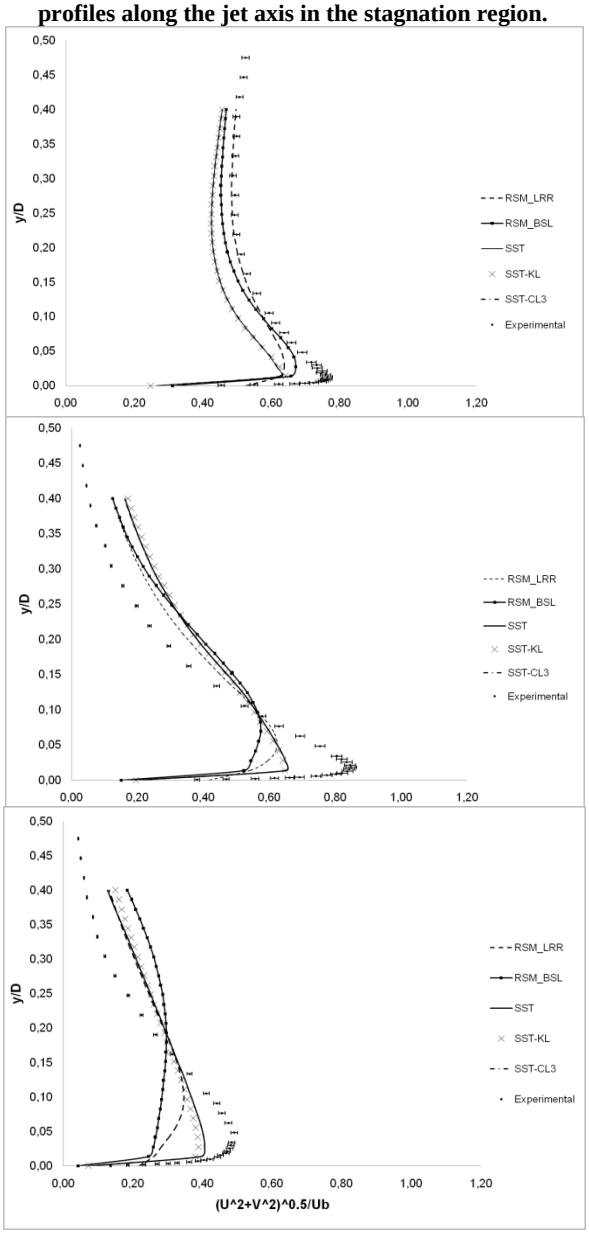

Figure 11. Mean velocity profiles of the wall-jet at r/D=0.5, r/D=1.5 and r/D=3.

Figure 12 shows the profiles of the r.m.s. of the axial/normal component of velocity at the same distances from the jet axis as in figure 11. Clearly, none of the tested turbulence models were able to capture the main experimental features. The RSM and the SST models return similar trends with differences only in the magnitude. Nonetheless, it is interesting to mention that for the two geometries investigated in this study, the maximum turbulence intensity remains of the order of 0,15 U_b whatever r/D.

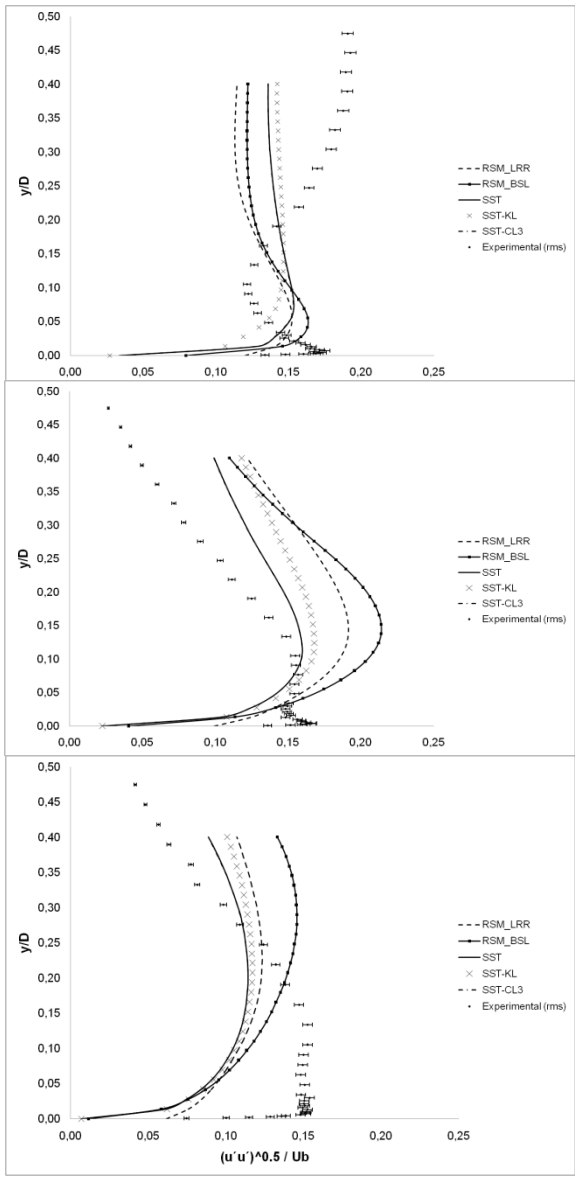

Figure 12. Development of the r.m.s. velocity fluctuation and Reynolds stress in the mean flow, for r/D=0,5; r/D=1,5 and r/D=3.

CONCLUSIONS

A comparison of the performance of five turbulence models to predict the dynamics of a round impinging jet in the wall region of the flow has been presented. Two RSM models were considered: a classic RSM and a RSM-BSL with a switching method based on ε and ω, and one two-equation model (SST) with two variants.

For H/D=2 and Re=2.3 10^4, the tested turbulence models predict mean velocity profiles in rather good agreement with experiments. The turbulent fields are not accurately computed. However, the inaccuracy of the numerical predictions is acceptable in view of the relevant low computational costs. The Kato-Launder´s modification of the SST model led to a good agreement with the experiments in comparison to the other SST and RSM models.

For H/D=6 and Re=7.0 10^4 good predictions are more difficult with all the turbulence models. While mean velocity fields are computed accurately, strong discrepancies exist between the computed and measured profiles of turbulent energy even though orders of magnitude seem to compare well.

The observed discrepancies for the latter can be attributed to the underlying formulations and modeling of turbulent viscosity, Reynolds stresses, and the use of wall functions.

Despite uncertainties in the inlet conditions used in the experiments, the SST models depicted a reasonable agreement with experiments in the impact zone along the jet axis line approaching the wall.

The SST model, with the Kato-Launder method to damp turbulent kinetic energy in stagnation zones, has proven to be a rather reliable approximation to compute impinging jets in engineering applications. It is important to notice that the RSM model with the ω formulation in the dissipation equation was not as successful as expected. It performed anyway much better than the classic RSM in this exercise.

REFERENCES

[1] Cooper D., Jackson, D.C., Launder, B.E. and Liao, G.X., 1993, "Impinging jet studies for turbulence model assessment. Part I: Flow-field experiments," *Int. J. Heat Mass Transfer*, vol. 36, pp. 2675-2684.

[2] Casey M. and Wintergerste T., 2000, "*Special Interest Group on "Quality and Trust in Industrial CFD" Best Practice Guidelines"*, European Research Community On Flow, Turbulence And Combustion (ERCOFTAC), version 1.

[3] Schlichting H., 1979, *Boundary Layer Theory*, McGraw Hill, E.E.U.U., Seventh Edition.

[4] Craft T., Graham L. and Launder B. 1993, "Impinging jet studies for turbulence model assessment. Part II An examination of the performance of four turbulence model," *Int. J. Heat Mass Transfer*, vol. 36, pp. 2685-2697.

[5] Dianat M., Fairweather M. and Jones W.P., 1996 "Reynolds Stress Closure Applied to Axisymmetric, Impinging Turbulent Jets," *Theoretical and Computational Fluid Dynamics*, vol. 8, pp. 435-447.

[6] Beaubert F. and Viazzo S., 2003, "Large eddy simulations of plane turbulent impinging jets at moderate Reynolds numbers," *Int. J. of Heat and Fluid Flow*, vol. 24, pp. 512-519.

[7] Rhea S., Bini M., Fairweather M. and Jones W.P., 2009, "RANS modeling and LES of a single-phase, impinging plane jet," *Computer and Chemical Engineering*, vol 33, pp. 1344-1353.

[8] Fernández J.A., Elicer-Cortés J.C., Valencia A., Pavageau M. and Gupta S., 2007, "Comparison of low-cost two-equation turbulence models for prediction flow dynamics in twin-jets devices," *Int. Communications in Heat and Mass Transfer*, vol. 34, pp. 570-578.

[9] Saddington A.J. and Knowles K., 2005, "A review of out-of-ground-effect propulsion-induced interference on STOVL aircraft," *Progress in Aerospace Sciences*, vol. 41, pp. 175-191.

[10] "*ANSYS CFX Reference Guide,"* 2009, release 12.0